Aggregation Effects on the Raman Spectroscopy of Dielectrophoretically Deposited Single-Walled Carbon Nanotubes

Lars M. Ericson and Pehr E. Pehrsson*

Naval Research Laboratory, 4555 Overlook Avenue, SW, Washington, DC 20375

Received: May 6, 2005; In Final Form: August 30, 2005

The effect of aggregation on surfactant-suspended individual single-walled carbon nanotube (SWNT) Raman spectroscopy has been explored in the context of dielectrophoretic separation. The Raman spectra of individual surfactant-suspended HiPco SWNTs deposited on a substrate and the same suspension deposited via dielectrophoresis were compared as a function of iterative aggregation states. The evolution of the samples' radial breathing modes and tangential modes at multiple excitation wavelengths (514, 633, and 785 nm) illustrates a direct correlation between changes in the Raman spectra and a broadening and downshifting of resonance transition energies. Dielectrophoresis samples exhibited Raman changes similar to control samples, indicating characterization of electronic separation is compromised by aggregation effects.

Introduction

Single-walled carbon nanotubes (SWNTs) are a unique material that has received tremendous attention since their discovery[1,2] due to their impressive electronic[3] properties. All known syntheses produce an ensemble of SWNT chiralities, and therefore a mixture of metallic and semiconducting nanotubes. To realize the full potential of SWNTs electronic applications, individual nanotubes of known electronic type must be separated, sorted, and assembled in a controlled fashion. Several SWNT separation schemes have been explored. Selective chemical reactivity has been used to preferentially functionalize metallic over semiconducting nanotubes, via both covalent chemistry[4] and ionic chemistry.[5] Column chromatography has been shown to be effective at separating DNA-wrapped nanotubes by electronic type by taking advantage of induced mirror charges in metallic nanotubes.[6] However, dielectrophoretic deposition has attracted notable attention recently because of its potential to combine directed assembly with electronic separation. Polarizable particles in suspension are subjected to an alternating electric field. Due to Coulomb interactions between the field and the induced dipole, the particle is either attracted or repulsed from regions of high field gradients. The direction of movement is determined by the relative dielectric constants of the particle and surrounding medium.[7] Dielectrophoresis has been used to deposit SWNTs between electrodes, with the degree of deposition and alignment dependent on the frequency and magnitude of the applied AC field.[8−12] In addition, Krupke et al. have reported selective deposition of metallic nanotubes over semiconducting ones, due to differences in the nanotube types' dielectric properties and the surrounding surfactant environment.[13] A metallic enrichment of 80% was suggested by Raman spectroscopy, with incomplete selectivity attributed to small amounts of metal-containing SWNT bundles remaining in suspension. However, Baik et al. recently reported attempts to selectively deposit metallic SWNTs using dielectrophoresis and attributed changes in Raman spectroscopy primarily to aggregation effects.[14]

Raman spectroscopy has often been the main analytical tool used to probe the efficacy of SWNT separation schemes, and the composition of SWNT solids. However, the effects of SWNT aggregation are rarely considered in the course of these analyses. Due to strong intertube coupling, aggregation has a dramatic effect on the band structure of SWNTs. According to theoretical studies, aggregation creates additional phonon dispersion along k_z and perpendicular to k_z, which respectively broadens and downshifts the transition energies involved in resonant Raman spectroscopy of SWNTs.[15] Reich et al., predict broadening of up to 200 meV and a 100 meV red shift.[16] Recent experimental studies confirm these effects and explore their ramifications for SWNT Raman spectroscopy.[17−19]

This paper examines the evolution of SWNT Raman spectroscopy as a function of aggregation. A consistent correlation between the behavior and changes in the Raman spectra for SWNT samples as a function of aggregation is explored. Results from a drop-dried reference sample are compared to Raman of samples prepared by using dielectrophoretic deposition in an effort to confirm metallic selectivity within the context of aggregation effects. Multiple excitation wavelengths allow monitoring of different SWNT transition energy regions.

Experimental Section

Raw HiPco SWNTs were suspended in 0.5 wt % aq sodium dodecyl benzene sulfonate (SDBS) and ultracentrifuged to isolate surfactant-stabilized individual SWNTs.[20] The suspension was drop-dried onto a silicon substrate with 100 nm thermal oxide for use as a reference sample (DD). Dielectrophoresis was performed with the same suspension and electrodes fabricated using conventional lithography. The electrodes possessed a 10 μm gap and were composed of 2 nm of titanium and 20 nm of gold deposited with electron beam evaporation onto silicon with the same 100 nm thermal oxide. A 10 μL drop of the SWNT suspension was placed on the electrodes and then 20 V peak-to-peak V_{ac} was applied at 3 MHz for 10 min. The sample (DEP1) was rinsed with deionized water (DI)

* Author to whom correspondence should be addressed. Mailing address: NRL Code 6176, 4555 Overlook Ave SW, Washington, DC, 20375. E-mail: pehrsson@ccs.nrl.navy.mil. Phone: 202-767-3579. Fax: 202-767-3321.

10.1021/jp052364p CCC: $30.25
Published on Web 10/07/2005

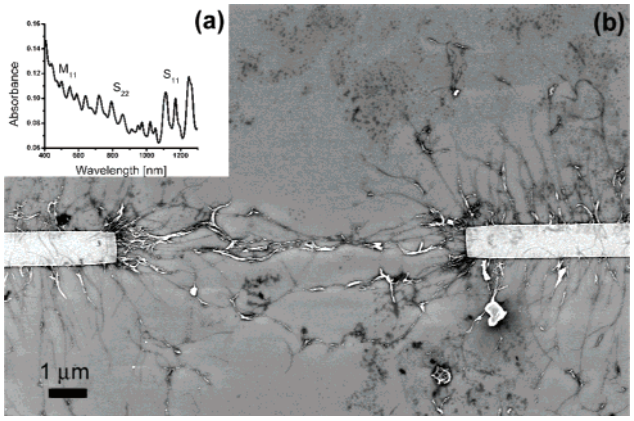

Figure 1. SWNT/SDBS suspension and DEP deposition. (a) Optical spectrum of surfactant-stabilized individual SWNTs with metallic and semiconductor transition regions labeled. (b) Scanning electron microscopy (SEM) image of Au electrodes after DEP1 nanotube deposition.

for 5 s, the function generator was then turned off, and the sample was rinsed again with ethanol for 5 s. Finally, the sample was dried under a light stream of nitrogen. Figure 1 depicts the electrode geometry and the resulting SWNT deposition of DEP1. A second sample (DEP2) was produced without any rinsing. The voltage was turned off and the drop of SWNT suspension lightly blown off. The dielectrophoresis conditions were chosen to be consistent with Krupke et al.'s experiments for comparison purposes.[13] Raman spectra were collected with a Renishaw Microraman 1000 with three excitation wavelengths: an Ar^+ laser at $\lambda_{exc} = 514$ nm (2.41 eV), a He−Ne at $\lambda_{exc} = 633$ nm (1.96 eV), and a diode laser at $\lambda_{exc} = 785$ nm (1.58 eV). The spot diameter was ∼1−2 μm and the laser polarization was parallel to the electrode gap.

Results and Discussion

Raman spectroscopy of the SWNT/SDBS suspension provides a starting reference with which to compare the aggregated samples (DD, DEP1, DEP2). The three excitation lasers allowed different subsets of SWNTs to be probed, covering a broad range of diameters and chiralities, including both metallic and semiconducting nanotubes. Figure 2 depicts the radial breathing modes (RBM) of the suspension and SWNT transition energies. Fantini et al. experimentally determined these transitions via analyses of Stokes and Anti-Stokes resonance windows of individual surfactant-suspended SWNTs over a wide range of excitation energies.[21] The intersection of the excitation laser and SWNT transitions energies determines the possible chiralities that one would expect to be in resonance with the lasers used, assuming no environmental perturbations. If the regions of interest are examined in closer detail a direct correlation can be made between the observed RBM peaks and specific SWNT transition energies. In addition, all chiralities resonant with the excitation lasers are within the expected 40−60 meV SWNT resonance window.[18] This supports the assumption that the suspension consists of individual surfactant-stabilized SWNTs whose RBM are not significantly influenced by their environment.

Raman spectroscopy of the DD sample yields different results. The suspension of individual SWNTs in SDBS was drop-dried and Raman spectra collected at multiple locations on the surface and averaged for each of the three excitation wavelengths. The sample was then soaked in DI (as opposed to rinsing, which involves a flowing stream of liquid) for a controlled length of

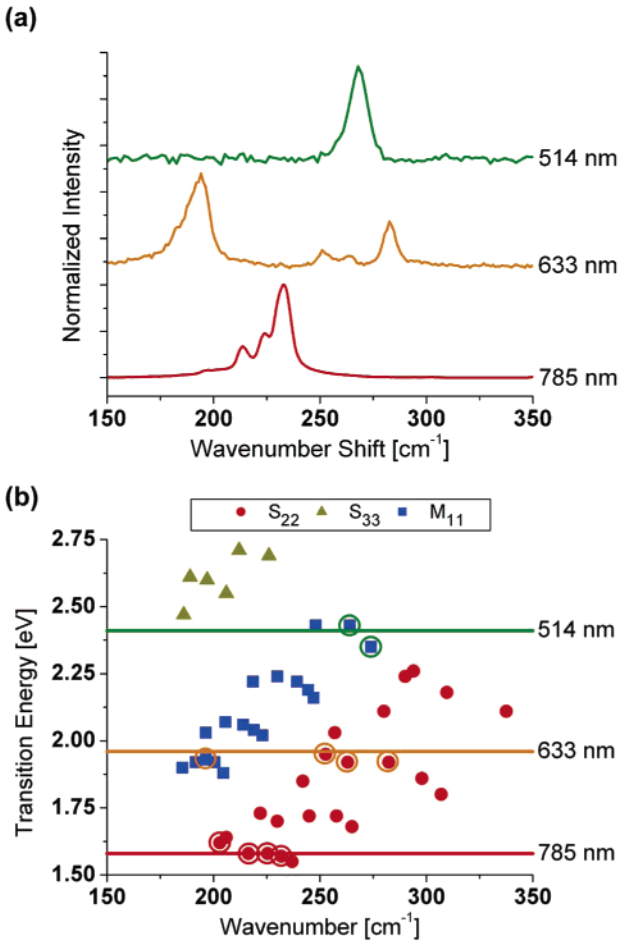

Figure 2. Resonant Raman spectra of SWNT/SDBS suspension. (a) RBM spectra at three wavelengths. Each spectrum is a composition of SWNTs in resonance with a given excitation energy. (b) Experimentally determined electronic transitions. Each laser is included as a horizontal line and each observed SWNT RBM is circled. All RBM are within the expected ∼40 meV SWNT resonance window.

time, removed, and lightly blown dry with nitrogen. Raman spectra were then collected. The process was repeated multiple times with increasing DI soaking durations. Figure 3 shows the RBM and tangential modes (TM) for the DD sample as a function of soaking iterations at $\lambda_{exc} = 514$ nm. Peaks that were previously not present in the suspension's Raman spectrum at 514 nm are prevalent, specifically the peak around 190 cm^{-1}. In addition, the relative intensities of the peaks change as a function of soaking. As the DD sample was soaked and dried, successively more surfactant was removed from the sample. The surfactant acted like a spatial insulator separating the individual nanotubes from one another. As the sample dried, capillary forces and van der Waals bonds increased the degree of aggregation.

Aggregation broadens the SWNT resonance windows and downshifts their transition energies due to strong intertube coupling.[16,18] These are the exact effects observed in the DD sample as a function of soaking. All of the peaks in Figure 3a−c correlate directly to transition energies in Figure 3d−f. For those energies to be resonant, the nanotube resonance windows must be significantly broadened from the original ∼40 meV, to as much as ∼200 meV in some cases. In addition, the evolution of the RBM at all three excitation wavelengths is explained by successively greater downshifting of the nanotubes' transition energies with increased aggregation. For $\lambda_{exc} = 514$ nm, the peaks around 260 cm^{-1} decrease in intensity relative to those

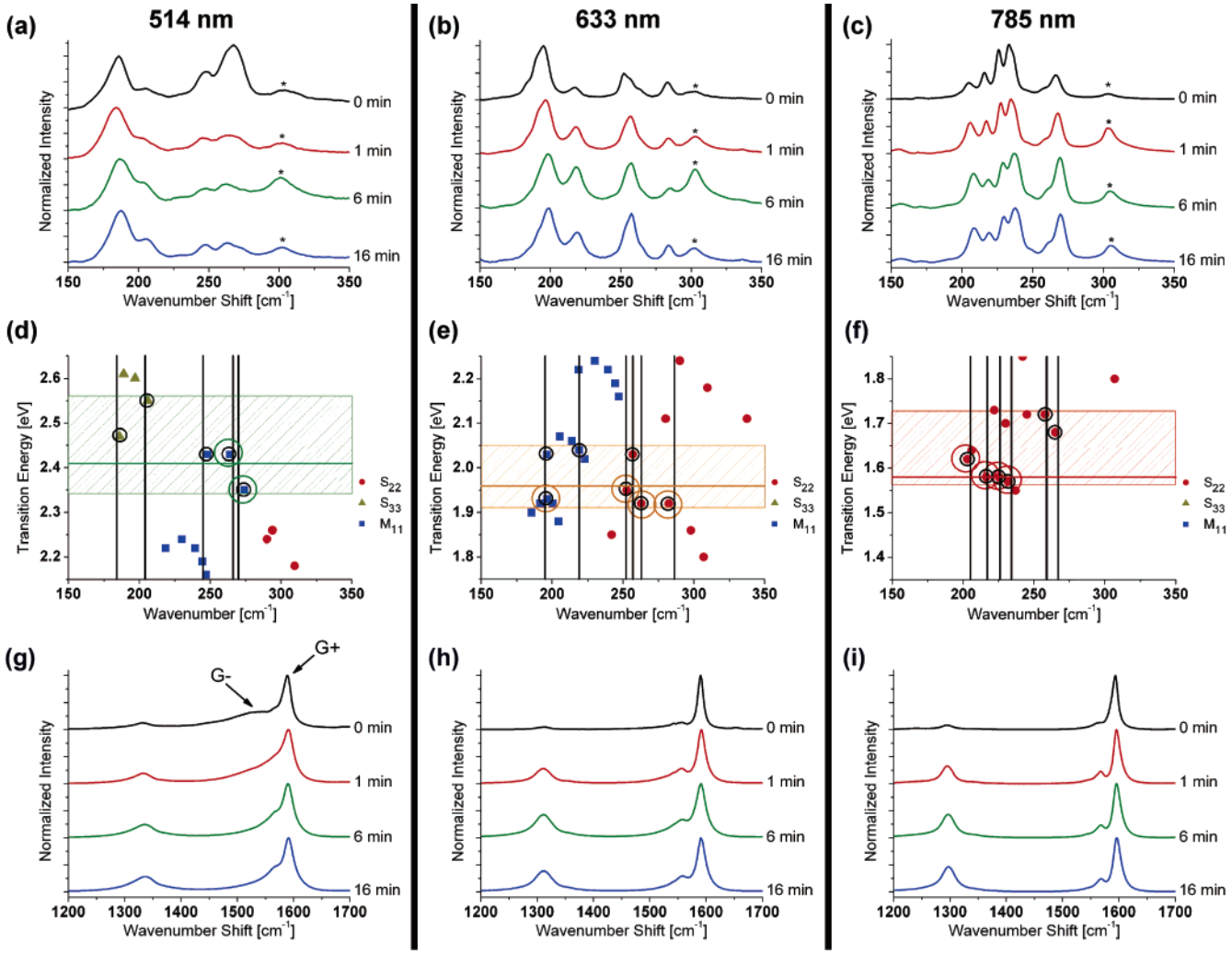

Figure 3. Raman spectroscopy of sample DD at three excitation wavelengths. (a−c) RBM spectra for the same sample as a function of varying iterative DI soaking times, normalized to peaks at 184, 195, and 234 cm^{-1}, respectively. The spectra show peaks not present in the liquid suspension and changes in relative intensity with increased aggregation. An asterisk denotes Si substrate peak. (d−f) Relevant electronic transition energies for each wavelength. Each point represents a transition energy for a given nanotube chirality. Vertical black lines have been added to draw attention to positions of peaks observed in the corresponding RBM spectrum directly above. Black circles highlight transitions observed in the aggregated sample, with colored circles indicting transitions observed in the liquid suspension (Figure 2). The shaded region outlines the minimum possible window required for all observed transitions to be in resonance. (g−i) Corresponding TM spectra for the three wavelengths. All data was taken on the same DD sample.

at ∼190 cm^{-1} (Figure 3a). The transitions originally in resonance (Figure 3d, green circles) downshift out of resonance and the 190 cm^{-1} transitions downshift into resonance. The TMs reflect this phenomenon (Figure 3g). The G$^-$ peak initially possesses a broader, lower frequency line shape characteristic of metallic SWNTs.[15] Aggregation makes the peaks more semiconductor-like; the G$^-$ peaks collapse and weaken with respect to the G$^+$ as the previously described RBM changes occur. In the case of λ_{exc} = 633 nm, the peaks at ∼220 and ∼260 cm^{-1} increase in intensity relative to the one around 190 cm^{-1} (Figure 3b). These changes are consistent with downshifting of the corresponding transitions (Figure 3e). The ∼220 cm^{-1} peak corresponds to a metallic transition not seen in the liquid SWNT/SDBS suspension, but due to aggregation it downshifts further into resonance. The TM corroborates this evolution (Figure 3h), with the G$^-$ line shape becoming more metallic as the metallic transitions at ∼220 cm^{-1} shift into resonance and some of the semiconducting transitions around 260 cm^{-1} shift partially out of resonance. The 260 cm^{-1} peak increases in intensity, but may also be misinterpreted as increasing in frequency. In reality, the peak is a composition of multiple RBM, which can be deconvoluted through comparison to the transition energies (Figure 3e). The increase in intensity and red shift in frequency is the result of the electronic transition corresponding to the central peak at 257 cm^{-1} downshifting into strong resonance with increased aggregation and the other two transitions shifting out of resonance, thus changing the shape and apparent location of the composition RBM. The RBM for λ_{exc} = 785 nm illustrates further examples of downshifted and broadened resonances. The peaks at ∼210 and ∼260 cm^{-1} intensify relative to the central cluster of peaks around 230 cm^{-1} (Figure 3c), consistent with downshifting of a broader subset of chiralities' transitions (Figure 3f). The peak at ∼210 cm^{-1} appears to red shift while increasing in intensity, but is again actually a composite of two RBMs in which the seemingly downshifting resonant transition corresponds to a second chirality with higher electronic transition frequency. The TM for 785 nm does not exhibit significant changes with aggregation, but this is expected because the probed chiralities before and after aggregation almost all correspond to semiconducting nanotubes.

In addition to exploring the evolution of the DD sample, the same analysis was applied to samples prepared with dielectrophoresis. In general, the RBM peaks for DEP1 are similar to

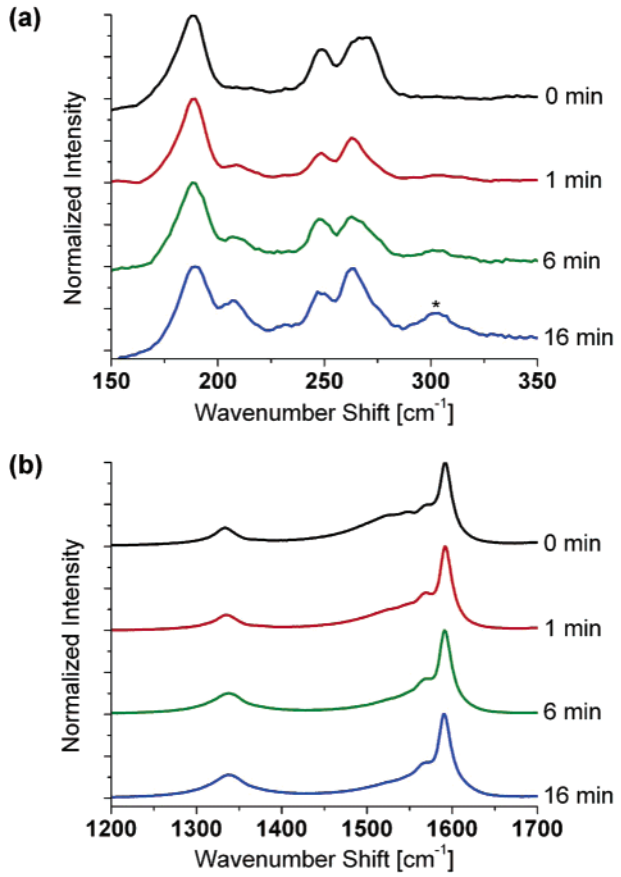

Figure 4. Raman spectroscopy of DEP1 at $\lambda_{exc} = 514$ nm. (a) RBM spectra at various iterative DI soaking steps (normalized to the 188 cm^{-1} peak) show possible minor metallic selectivity. The asterisk denotes the Si substrate peak. (b) Corresponding TM spectra show little metallic enhancement over sample DD and do not support selectivity.

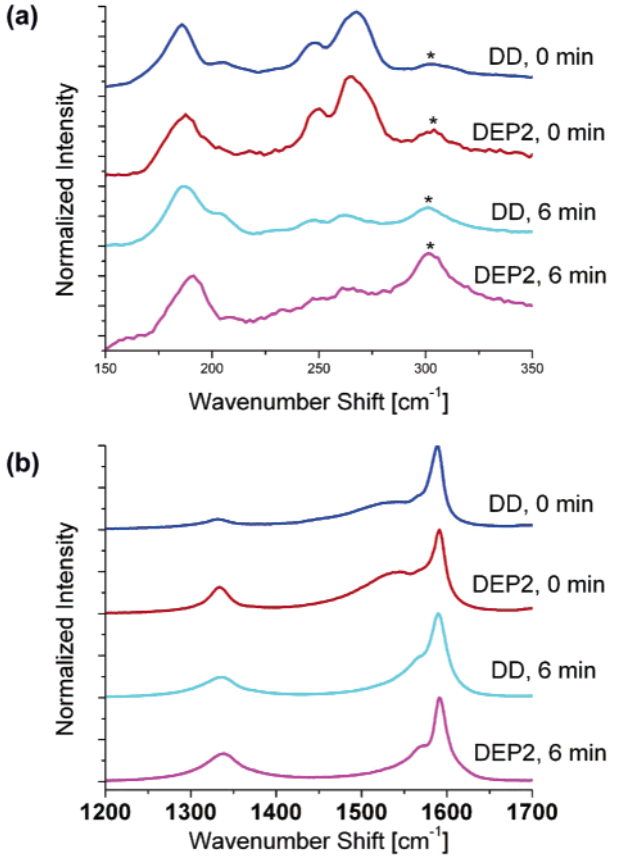

Figure 5. Comparison of DD and DEP2 before and after DI soaking at $\lambda_{exc} = 514$ nm. (a) RBM spectra show DD and DEP2 to have similar intensities before and after increased aggregation, normalized to the 185 cm^{-1} peak. An asterisk denotes the Si substrate peak. (b) Corresponding TM confirm similar composition and behavior.

DD, in that peaks are observed that were previously absent in the liquid suspension's Raman spectrum and the relative intensities of the peaks change with increased aggregation (Figure 4a). The grouping of peaks around 260 cm^{-1} (metallic transitions, Figure 3d) does not exhibit the dramatic reduction in intensity relative to the semiconductor RBM peaks around 190 cm^{-1} (semiconductor transitions, Figure 3d) observed for DD. This difference could suggest a preferential deposition of metallic nanotubes by dielectrophoresis. However, the corresponding TM does not exhibit a strong metallic G^- peak (Figure 4b). In addition, if dielectrophoresis selectively deposited metallic nanotubes under the conditions used, as has been reported elsewhere,[13] one would expect the semiconducting peak at ~190 cm^{-1} to be absent or dramatically reduced in intensity. Spectra taken for DEP1 at 633 and 785 nm show similar results—possible minor enhancement of metallic RBM peaks (Supporting Information) compromised by dominant aggregation effects.

To further explore the effects of aggregation on dielectrophoretic samples, DEP2 was prepared without any initial rinsing during sample preparation. The resulting sample provides a closer comparison to DD, but deviates from the protocol used by other research groups.[13] The resulting RBM and TM spectra at $\lambda_{exc} = 514$ nm show good agreement (Figure 5). The RBM of both samples are initially dominated by the group of metallic peaks around 260 cm^{-1}, but after two soaking (and aggregation) cycles the semiconducting peak at ~190 cm^{-1} increases in intensity to several times that of the metallic peaks. These changes, as explained previously for DD, are consistent in the context of the transition energies. The TM of DEP2 is initially more metallic, but after the same soaking and aggregation cycles, both collapse to the same aggregated line shape. A difference in SWNT density or starting aggregation is most likely the cause of DEP2's more metallic line shape at the beginning, which is reasonable given the different methods of deposition.

Every effort was taken to reproduce the selective dielectrophoretic deposition reported by Krupke et al. Deposition from suspensions of SWNT/SDBS in D_2O yielded similar results, and repeated depositions using the methods described herein were consistent. Dimaki et al. recently reported SWNT dielectrophoresis simulations under various conditions and suggested frequencies above 200 MHz would be necessary for selective deposition.[22] However, the results of these experiments corroborate Baik et al.'s findings[14] and do not unequivocally support dielectrophoretic separation as determined by Raman spectroscopy, instead indicating that aggregation effects can dominate such analyses.

Conclusion

The evolution of SWNT Raman spectra was explored as a function of aggregation at multiple wavelengths. A direct correlation of the changes in the Raman spectra to experimentally determined transition energies confirms that SWNT aggregation significantly broadens and downshifts the transition energies. The results did not conclusively demonstrate that dielectrophoretic deposits were selectively enriched in metallic nanotubes, and emphasizes the need to consider aggregation effects in interpreting the Raman spectra. Dielectrophoresis may

still prove to cause selective deposition, but this research shows that aggregation plays an important role in the apparent metallic to semiconductor SWNT ratios and can significantly compromise conclusions based on Raman alone. Raman must be combined with additional analytical methods, such as electrical characterization, chemical reactivity, and absorption spectroscopy, to quantify the efficacy of SWNT separation. We will present such combined studies in future papers.

Acknowledgment. This work was supported by a grant from the Defense Threat Reduction Agency (AA04DET004). This research was performed while L. Ericson held a National Research Council Research Associateship Award at the Naval Research Laboratory.

Supporting Information Available: Additional Raman spectroscopy of DEP1 at $\lambda_{exc} = 633$ and 785 nm. This material is available free of charge via the Internet at http://pubs.acs.org.

References and Notes

(1) Bethune, D. S.; Kiang, C. H.; de Vries, M. S.; Gorman, G.; Savoy, R.; Vasques, J.; Beyers, R. *Nature* **1993**, *363*, 605.

(2) Ebbesen, T. W.; Ajayan, P. M. *Nature* **1992**, *358*, 220.

(3) Tans, S. J.; Devoret, M. H.; Dai, H.; Thess, A.; Smalley, R. E.; Geerligs, L. J.; Dekker, C. *Nature* **1997**, *386*, 474.

(4) Strano, M. S.; Dyke, C. A.; Usrey, M. L.; Barone, P. W.; Allen, M. J.; Shan, H.; Kittrell, C.; Hauge, R. H.; Tour, J. M.; Smalley, R. E. *Science* **2003**, *301*, 1519.

(5) Chen, Z.; Du, X.; Du, M. H.; Rancken, C. D.; Cheng, H. P.; Rinzler, A. G. *Nano Lett.* **2003**, *3*, 1245.

(6) Zheng, M.; Jagota, A.; Strano, M. S.; Santos, A. P.; Barone, P.; Chou, S. G.; Diner, B. A.; Dresselhaus, M. S.; Mclean, R. S.; Onoa, G. B.; Samsonidze, G. G.; Semke, E. D.; Usrey, M.; Walls, D. J. *Science* **2003**, *302*, 1545.

(7) Green, N. G.; Ramos, A.; Morgan, H. *J. Phys. D* **2000**, *33*, 632.

(8) Chen, X. Q.; Saito, T.; Yamada, H.; Matsushige, K. *Appl. Phys. Lett.* **2001**, *78*, 3714.

(9) Nagahara, L. A.; Amlani, I.; Lewenstein, J.; Tsui, R. K. *Appl. Phys. Lett.* **2002**, *80*, 3826.

(10) Krupke, R.; Hennrich, F.; Weber, H. B.; Beckmann, D.; Hampe, O.; Malik, S.; Kappes, M. M.; Lohneysen, H. V. *Appl. Phys. A* **2003**, *76*, 397.

(11) Li, J.; Zhang, Q.; Yang, D.; Tian, J. *Carbon* **2004**, *42*, 2263.

(12) Suehiro, J.; Zhou, G.; Hara, M. *J. Phys. D* **2003**, *36*, L109.

(13) Krupke, R.; Hennrich, F.; Kappes, M. M.; Lohneysen, H. V. *Nano Lett.* **2004**, *4*, 1395.

(14) Baik, S.; Usrey, M.; Rotkina, L.; Strano, M. *J. Phys. Chem. B* **2004**, *108*, 15560.

(15) Dresselhaus, M. S.; Eklund, P. C. *Adv. Phys.* **2000**, *49*, 705.

(16) Reich, S.; Thomsen, C.; Ordejon, P. *Phys. Rev. B* **2002**, *65*, 155411.

(17) O'Connell, M. J.; Sivaram, S.; Doorn, S. K. *Phys. Rev. B* **2004**, *69*, 235415.

(18) Heller, D. A.; Barone, P. W.; Swanson, J. P.; Mayrhofer, R. M.; Strano, M. S. *J. Phys. Chem. B* **2004**, *108*, 6905.

(19) Strano, M. S.; Moore, V. C.; Miller, M. K.; Allen, M. J.; Haroz, E. H.; Kittrell, C.; Hauge, R. H.; Smalley, R. E. *J. Nanosci. Nanotechnol.* **2003**, *3*, 81.

(20) O'Connell, M. J.; Bachilo, S. M.; Huffman, C. B.; Moore, V. C.; Strano, M. S.; Haroz, E. H.; Rialon, K. L.; Boul, P. J.; Noon, W. H.; Kittrell, C.; Ma, J.; Hauge, R. H.; Weisman, R. B.; Smalley, R. E. *Science* **2002**, *297*, 593.

(21) Fantini, C.; Jorio, A.; Souza, M.; Strano, M. S.; Dresselhaus, M. S.; Pimenta, M. A. *Phys. Rev. Lett.* **2004**, *93*, 147406.

(22) Dimaki, M.; Boggild, P. *Nanotechnology* **2004**, *15*, 1095.